Research paper

Theoretical study on the optical emission processes in geminally locked tetraphenylethylene derivatives

Tian Zhang[a,*], Guozheng Zhu[a], Lili Lin[b], Jianzhong Fan[b], Guangshuai Gong[a], Jinglin Mu[a], Ling-Bao Xing[a], Yujun Xie[c], Shuping Zhuo[a,**]

[a] *School of Chemistry and Chemical Engineering, Shandong University of Technology, Zibo 255049, PR China*
[b] *Shandong Province Key Laboratory of Medical Physics and Image Processing Technology, Institute of Materials and Clean Energy, School of Physics and Electronics, Shandong Normal University, Jinan 250014, PR China*
[c] *Institute of Molecular Aggregation Science, Tianjin University, Tianjin 300072, PR China*

HIGHLIGHTS

- The excited-state dynamics of several geminally locked TPE derivatives have been theoretically investigated.
- The emission quantum efficiency is predicted to increase in the order of 2ETPE ≪ 2MTPE ≈ 2STPE < 2OTPE.
- Electron-vibration coupling results indicate that the out-of-plane vibrations are restricted with strengthening the tethers.

ARTICLE INFO

ABSTRACT

We theoretically investigate the excited-state dynamics of several geminally locked tetraphenylethylene (TPE) derivatives in solution, to explore the relationship between bridged structures and their respective luminescent properties. The emission of 2ETPE is found to be weak due to the largest non-radiative decay rate with 9 orders of magnitude. Conversely, the favorable better conjugation induced by lone pairs and stronger rigidity provides 2OTPE with brightest emission. The competition between the enhanced conjugation and attenuated rigidity of 2STPE in comparison with 2MTPE result in their moderate emission. This work provides strategy for tuning the emission of the TPE derivatives via varying tethers.

1. Introduction

Tetraphenylethylene (TPE) and its derivatives have attracted considerable interest for their colossal applications in the fields of organic light-emitting, chemo/biosensing and stimuli response [1–3]. The easy synthesis and modification have turned them into the most studied architectures with the aggregation-induced emission (AIE) character. AIE-active luminogens (AIEgens) are weak or non-emissive in solution but emit strong light upon aggregation [4]. TPE is an archetypal AIEgen but the luminescence properties of its derivatives are strongly structure-dependent. Among varieties of functionalized TPE derivatives, the geminally locked ones with two tethers between geminal phenyl groups arouse our curiosity. The ethylene ($-CH_2-CH_2-$) tethered TPE (2ETPE) shows almost no fluorescence in tetrahydrofuran (THF) with the fluorescence quantum yield (Φ_f) as low as 0.1% [5,6], but the oxygen ($-O-$) bridged TPE (2OTPE) emits brightly (Φ_f = 30.1%) [7].

The optical property of 2OTPE is remarkably different from 2ETPE although the TPE units are both locked. The rigidity of the tethers might account for the distinctive fluorescence. From this point of view, we designed the methylene ($-CH_2-$) tethered TPE (2MTPE) and the sulfur ($-S-$) bridged TPE (2STPE) via varying degrees of rigidity. Both 2MTPE and 2STPE were early synthesized [8,9] but their fluorescence behaviors are still unknown. The primary purpose of this work is to investigate the excited-state dynamics of these systems at the first-principles level and explore the relationship between the bridged structures and their respective luminescent properties.

Herein, we carried out computational investigations on the optical emission processes of 2ETPE, 2MTPE, 2STPE and 2OTPE (Fig. 1) in solution. The polarizable continuum model (PCM) was used to mimic the solvent environment. The thermal vibrational correlation function (TVCF) formalism was applied to compute the optical spectra and excited-state decay rate constants. Our theoretical study gains deeper

---

* Corresponding author.
** Corresponding author.
E-mail addresses: tzhang@sdut.edu.cn (T. Zhang), zhuosp_academic@yahoo.com (S. Zhuo).
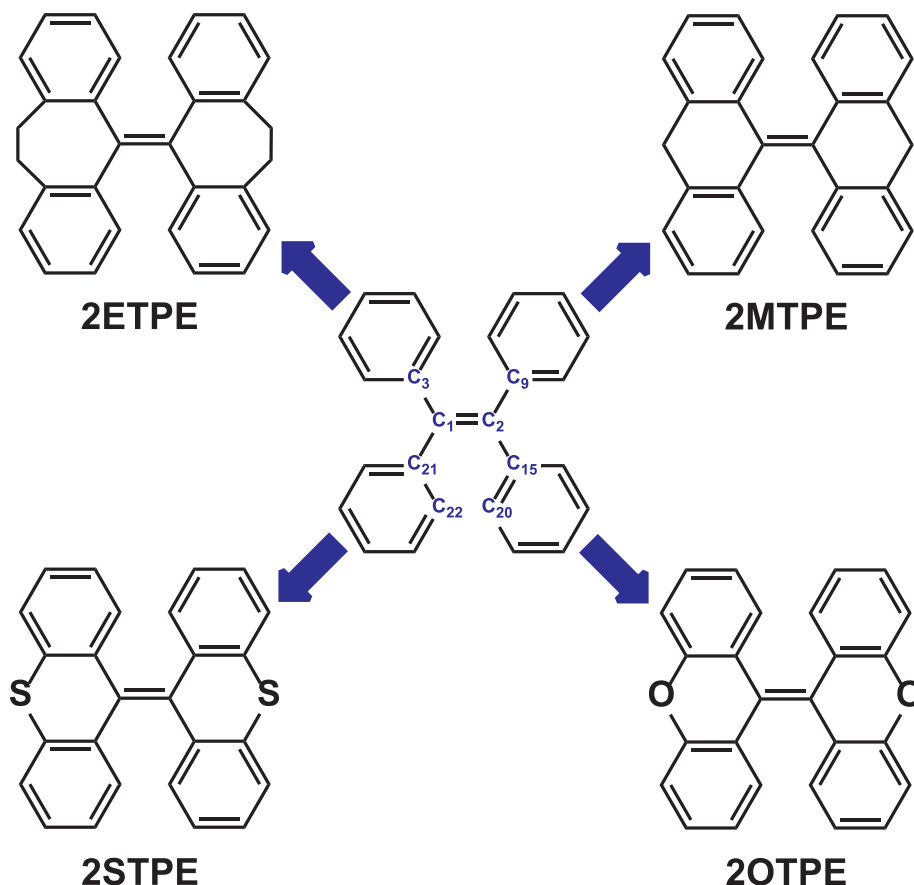
Fig. 1. Molecular structures of 2ETPE, 2MTPE, 2STPE and 2OTPE.

insight into the effect of varying tethers at *gem*-positions on the emission quantum efficiency of the TPE derivatives.

2. Theoretical methods

Geometry optimizations and electronic structure calculations were performed for the ground (S_0) state by using density functional theory (DFT) and for the first singlet excited (S_1) state by employing time-dependent DFT (TD-DFT). The PBE0 [10] functional together with 6-31G(d) basis set was adopted, which has been benchmarked to be a reliable level for description of the singlet excited states [11]. The solvent effect was taken into account through the PCM implemented in the Gaussian 16 package [12]. The THF solution was chosen in consistent with the experiment. The equilibrium solvation method [13] was applied in both geometry optimizations and frequency calculations. The state-specific solvation approach [14] was used to compute the vertical transition properties. Light-emitting process is dictated by the competition between the radiative and non-radiative decay. The Φ_f is determined by the equation of $k_r/(k_r + k_{nr})$. k_r is the radiative decay rate. k_{nr} includes the internal conversion rate (k_{ic}) and intersystem crossing rate (k_{isc}). k_{isc} can be ignored due to the negligible spin-orbit coupling (SOC) for most organic molecules with $^1(\pi, \pi^*) \rightarrow {}^3(\pi, \pi^*)$ transition character [15]. Based on the electronic structure and Hessian information of the S_0 (S_1) states, we calculated the vibrationally resolved optical spectra, k_r and k_{ic} with the help of the MOMAP [16].

The analytical formalism [17] we applied to obtain the absorption and emission spectra can be written as:

$$\sigma_{ab}^{FC}(\omega, T) = \frac{2\pi\omega}{3\hbar c} |\vec{\mu}_0|^2 \int_{-\infty}^{\infty} e^{i(\omega-\omega_{fi})t} Z_i^{-1} \rho_{ab,0}^{FC}(t, T)dt \tag{1}$$

$$\sigma_{em}^{FC}(\omega, T) = \frac{2\omega^3}{3\pi\hbar c^3} |\vec{\mu}_0|^2 \int_{-\infty}^{\infty} e^{-i(\omega-\omega_{if})t} Z_i^{-1} \rho_{em,0}^{FC}(t, T)dt \tag{2}$$

where $\vec{\mu}_0$ is an electric transition dipole moment constant under the Franck-Condon approximation and Z_i is the partition function. $\rho_{ab,0}^{FC}(t, T)$ and $\rho_{em,0}^{FC}(t, T)$ are the correlation functions and $\rho_{ab,0}^{FC}(t, T) = \rho_{em,0}^{FC}(t, T) = \text{Tr}[e^{-i\tau_f \hat{H}_f} e^{-i\tau_i \hat{H}_i}]$.

The analytical formalism [17,18] of k_r and k_{ic} can be expressed as:

$$k_r(T) = \int \sigma_{em}^{FC}(\omega, T)d\omega \tag{3}$$

$$k_{ic}(T) = \sum_{kl} \frac{1}{\hbar^2} R_{kl} \int_{-\infty}^{\infty} [e^{i\omega_{if}t} Z_i^{-1} \rho_{ic,kl}(t, T)]dt \tag{4}$$

where $\rho_{ic,kl}(t, T)$ is the correlation function and $\rho_{ic,kl}(t, T) = \text{Tr}(\hat{P}_{fk} e^{-i\tau_f \hat{H}_f} \hat{P}_{fl} e^{-i\tau_i \hat{H}_i})$. The non-adiabatic electronic couplings related to R_{kl} were computed through the first-order perturbation theory following Lin [19].

3. Results and discussion

3.1. Electronic structure and transition energy

As shown in the previous investigations [6,7,20–22], the emission properties of TPE derivatives are closely related to the twist of C=C bond and the rotation of phenyl rings. Therefore, we presented the corresponding bond lengths and dihedral angles (Fig. 1) in Table 1, with the geometric parameters at the S_0/S_1 minimum and their changes. It can be seen that both the lengths of the central C=C bond (C_1-C_2) and its connected single bond (C_2-C_{15}) exhibit tiny variations upon excitation for the investigated TPE derivatives. C_1-C_2 elongates ~ 0.10 Å and C_2-C_{15} shortens ~ 0.04 Å. However, the torsional motions around these double and single bonds are significant. C_{21}-C_1-C_2-C_{15} and

Table 1
Selected bond lengths (in Å) and dihedral angles (in deg) of 2ETPE, 2MTPE, 2STPE and 2OTPE at the S_0/S_1 minimum in solution. Δ represents the structural change between the optimized S_0 and S_1 states.

	S_0	S_1	Δ	S_0	S_1	Δ	S_0	S_1	Δ	S_0	S_1	Δ
	2ETPE			2MTPE			2STPE			2OTPE		
C_1-C_2	1.36	1.46	0.10	1.36	1.45	0.09	1.36	1.44	0.08	1.36	1.45	0.09
C_2-C_{15}	1.50	1.46	0.04	1.49	1.45	0.04	1.48	1.45	0.03	1.48	1.45	0.03
C_{21}-C_1-C_2-C_{15}	4.93	15.25	10.32	−0.78	9.63	10.41	0.12	11.06	10.94	−2.50	5.84	8.34
C_1-C_2-C_{15}-C_{20}	52.50	34.26	18.24	47.59	33.46	14.13	50.22	34.51	15.71	42.92	31.51	11.41

C_1-C_2-C_{15}-C_{20} show great changes of ~10° and 11–18°, respectively. The modification of C_{21}-C_1-C_2-C_{15} follows the order of 2ETPE ≈ 2MTPE ≈ 2STPE > 2OTPE and that of C_1-C_2-C_{15}-C_{20} decreases in the order of 2ETPE > 2STPE > 2MTPE > 2OTPE. Therefore, the structural rigidity can be quantified and increases in the order of 2ETPE < 2STPE < 2MTPE < 2OTPE. The more flexible structure implies faster geometry relaxations in the $S_1 \rightarrow S_0$ internal conversion process.

Calculated vertical transition energies (ΔE_{vert}) at the S_0 and S_1 equilibrium geometries, electric transition dipole moments (μ) and oscillator strengths (f) are listed in Table 2. The calculated transition energies well reproduce the peak values of the experimental optical spectra with the largest deviation being 0.17 eV. We can see that the absorption peaks are obviously red-shifted from 2ETPE to 2MTPE after that 2STPE finally 2OTPE, whereas the emission peaks exhibit firstly a remarkable red-shift from 2ETPE to 2MTPE but then slight shifts from 2MTPE to 2STPE finally 2OTPE. Table 2 also shows that their strong-dipole allowed transitions (large μ and f) are mostly HOMO → LUMO with the assignments of > 98%. The electron density contours of HOMOs and LUMOs as well as their energy levels are shown in Fig. 2. The HOMOs and LUMOs mainly demonstrate π and π^* character, respectively. The HOMO-LUMO energy gaps at their S_0 equilibrium geometries follow the order of 2ETPE > 2MTPE > 2STPE > 2OTPE, in accord with the absorption maxima energies in that order. The gaps are dominated by the structural twisting degree and conjugation extent. The former opens the gaps and the latter narrows the gaps with the enhancement. Through comparative analysis of the absolute values of C_{21}-C_1-C_2-C_{15} and C_1-C_2-C_{15}-C_{20} at S_0/S_1-geometries for these systems (Table 1), we found all of them possess twisted structures. The structural twisting degree decreases generally in the order of 2ETPE > 2STPE > 2MTPE > 2OTPE, in line with that of the tether lengths −CH$_2$−CH$_2$− (4.55 Å) > −S− (3.55 Å) > −CH$_2$− (3.02 Å) > −O− (2.75 Å). Textbook knowledge tells us that the sulfur/oxygen atom in 2STPE/2OTPE has the lone pair conjugated to adjacent π-electron phenyls, which decreases the LUMO level and increases the conjugation [23]. So the conjugation extent is greater for 2STPE and 2OTPE compared to 2ETPE and 2MTPE. Therefore, the gap of 2ETPE is largest due to the most twisted and less conjugated structure. The better conjugation of 2STPE than 2MTPE overwhelms the gap opening caused by its
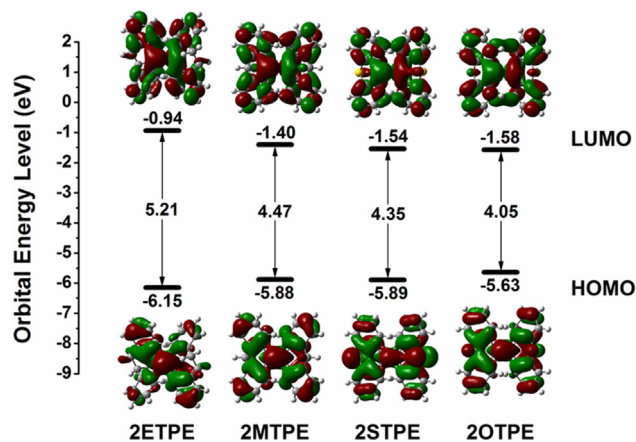

Fig. 2. Calculated energy levels, energy gaps and electron density contours of the HOMOs and LUMOs for 2ETPE, 2MTPE, 2STPE and 2OTPE at their S_0 equilibrium geometries in solution.

more twisting degree and narrows the gap. The least twisted and more conjugated skeleton of 2OTPE result in the smallest gap.

3.2. Excited-state radiative and non-radiative decay rate constants

Calculated and available experimental optical spectra are shown in Fig. 3. The calculated vibrationally resolved spectra of 2ETPE and 2OTPE agree well with the existing experiments, which validate the TVCF formalism coupled with PCM method adopted in this work. Note that the spectra lineshapes naturally originate from the temperature effect and vibronic structure without any broadening. The broken mirror symmetry between the absorption and emission spectra arises from the distortion effect between the S_0 and S_1 potential energy parabolas [24]. The shifts of the spectra are similar to the calculated vertical transition energies. The occurrence and enhancement of the vibronic feature in the emission spectra implies more rigid structure.

Calculated k_r, k_{ic} and Φ_f are listed in Table 3. The Lorentz broadening width (FWHM) of 10.60 cm^{-1} is included in the k_{ic} calculations to ensure unity and convergence of the correlation function following
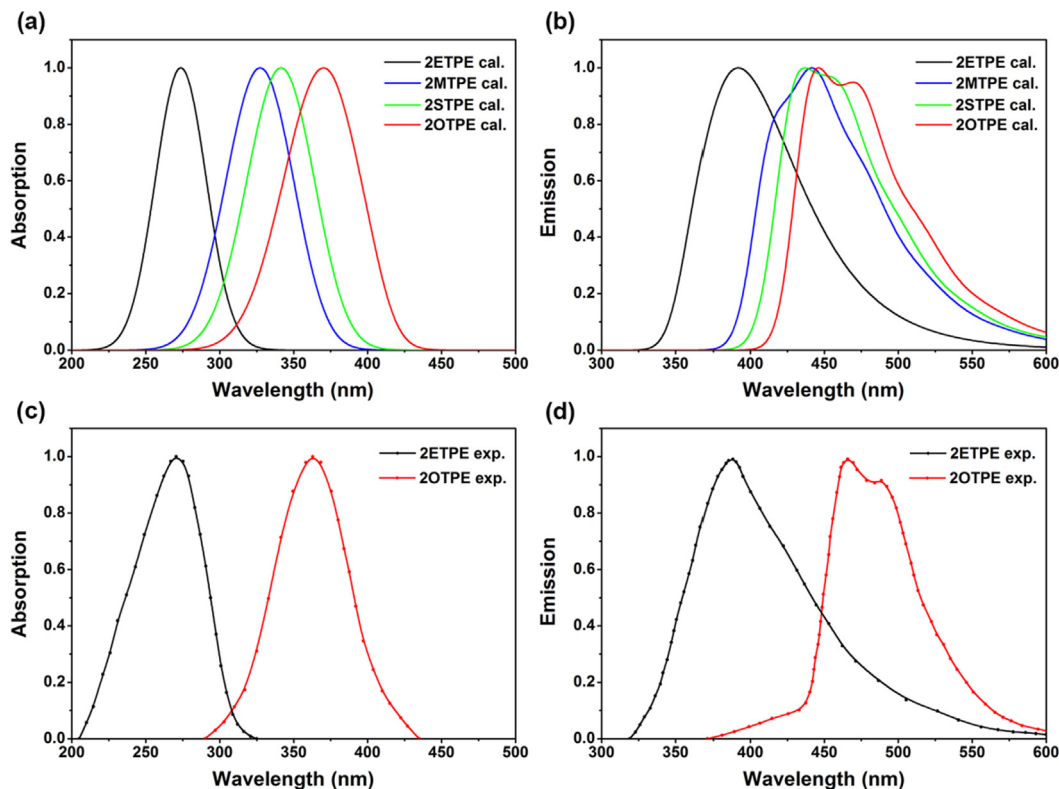
Table 2
Calculated vertical transition energies (ΔE_{vert}), electric transition dipole moments (μ), oscillator strength (f) and HOMO → LUMO assignments for 2ETPE, MTPE, 2STPE and 2OTPE in solution. Available experimental (exp.) peak values are also given for comparison.

		ΔE_{vert}	exp.	μ	f	HOMO → LUMO
2ETPE	Absorption	4.46 eV (278 nm)	4.63 eV (268 nm)[a]	4.86 D	0.40	98.1%
	Emission	3.11 eV (399 nm)	3.19 eV (389 nm)[a]	5.31 D	0.33	98.7%
2MTPE	Absorption	3.80 eV (326 nm)	N. A.	5.18 D	0.39	98.8%
	Emission	2.74 eV (453 nm)	N. A.	5.36 D	0.30	99.0%
2STPE	Absorption	3.59 eV (345 nm)	N. A.	4.17 D	0.24	97.0%
	Emission	2.68 eV (463 nm)	N. A.	5.54 D	0.31	98.8%
2OTPE	Absorption	3.40 eV (365 nm)	3.40 eV (365 nm)[b]	5.40 D	0.38	98.2%
	Emission	2.63 eV (471 nm)	2.66 eV (466 nm)[b]	5.71 D	0.32	98.8%

[a] In THF [6].
[b] In THF [7].

Fig. 3. Calculated (cal.) absorption (a) and emission (b) spectra for 2ETPE, 2MTPE, 2STPE and 2OTPE, as well as experimental (exp.) absorption (c) and emission (d) spectra for 2ETPE and 2OTPE in solution ($T = 298$ K).

Table 3
Calculated k_r (s^{-1}), k_{ic} (s^{-1}) and Φ_f for 2ETPE, 2MTPE, 2STPE and 2OTPE in solution ($T = 298$ K). Available experimental Φ_f values are also presented in parentheses.

	k_r	k_{ic}	Φ_f
2ETPE	1.3×10^8	1.8×10^9	6.7% (0.1%)
2MTPE	8.7×10^7	9.1×10^7	48.9% (N.A.)
2STPE	9.4×10^7	9.4×10^7	50.0% (N.A.)
2OTPE	9.1×10^7	6.2×10^7	59.5% (30.1%)

Niu [17]. The Einstein spontaneous emission relationship tells us k_r is proportional to the oscillator strength and vertical transition energy in the emission process, $k_r \sim f \Delta E_{vert}^2$. Therefore, the k_r value of 2ETPE is largest due to the hypsochromic vertical emission energy than others (Table 2 and Fig. 3). The k_r values of 2STPE and 2OTPE are slightly larger than 2MTPE because of the lone-pair conjugation induced greater f and minor-shifted ΔE_{vert}. k_{ic} decreases in the order of 2ETPE > 2STPE > 2MTPE > 2OTPE, in consistent with the increase order of the structural rigidity. Φ_f can be expressed as $\Phi_F \approx k_r/(k_r + k_{ic})$, and either increase k_r or decrease k_{ic} could achieve high Φ_f. The calculated Φ_f value (6.7%) of 2ETPE is smallest because its k_{ic} value is largest with 9 orders of magnitude, overwhelming the still greater k_r. 2OTPE becomes brightest ($\Phi_f = 59.5\%$) owing to its slowest k_{ic} and moderate k_r. Although both Φ_f values of 2ETPE and 2OTPE are overestimated because the possible formation of photocyclized intermediate has not been considered [6,20], the experimentally distinctive luminescence fact between dark 2ETPE and bright 2OTPE is expected. Both ordinary and competitive k_r and k_{ic} result in the moderate and similar Φ_f (~50%) of 2STPE and 2MTPE.

3.3. Projection of the reorganization energy onto mode and geometry relaxations

To gain deeper insight into the non-radiative decay process, we project the total reorganization energy $\lambda_{g(e)}$ onto both mode and geometry relaxations. $\lambda_{g(e)}$ quantifies the intramolecular vibrational relxations in the ground-state (excited-state) potential energy surface (PES), which demonstrates the vibrations' ability to accept the excited-state electronic energy. Based on the harmonic oscillator approximation, the λ_j of each normal mode is defined as its energy $\hbar \omega_j$ times Huang-Rhys factor S_j, $\lambda_j = \hbar S_j \omega_j = \frac{1}{2} D_j^2 \omega_j^2$. D_j is the displacement along the j-th normal mode between two electronic states. The aggregation of all normal modes is the total, *i.e.*, $\lambda_{g(e)} = \sum_{j \in g(e)} \lambda_j$ [25]. λ_j versus ω_j in the ground-state PES is depicted in Fig. 4a, as well as displacement vectors of significant modes with large λ_j. Note that either using λ_j in λ_g or that in λ_e could draw the same conclusion, as illustrated in our previous study [26]. The normal-mode analyses were done in the EVC module embedded in the MOMAP program. It can be seen that λ_j in two vibration regions, low-frequency (LF, < 200 cm^{-1}) and high-frequency (HF, 1600–1800 cm^{-1}), are major consumption channels in the non-radiative energy relaxation process. The contribution of all LF modes to the total is 37.1% (250 meV) in 2ETPE, whereas it decreases to 33.6% (149 meV) in 2STPE, 27.3% (135 meV) in 2MTPE and 24.0% (87 meV) in 2OTPE, respectively. However, the contribution of all HF modes experiences minor modification compared to the LF modes. This indicates that the non-radiative energy dissipation channels via LF modes are gradually deactivated with strengthening the tethers. S_j versus ω_j is also shown in Fig. 4b, which characterizes the electron-vibration coupling strength of the j-th normal mode. It is more straightforward that S_j of the LF modes decrease in the order of 2ETPE > 2STPE > 2MTPE > 2OTPE, whereas S_j of the HF modes are trivial. Therefore, the largely reduced λ_j of the LF modes mainly stems from the decreased S_j, slowing down the k_{ic} in that order. The LF modes are mainly assigned to the out-of-plane motions, *e.g.*, twisting vibration in 2ETPE, rocking
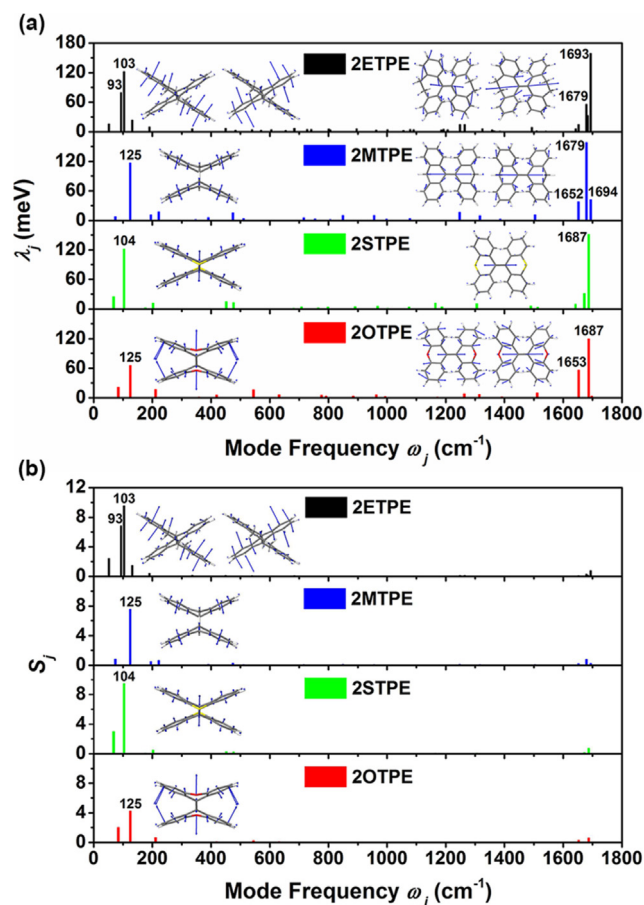
Fig. 4. Reorganization energy λ_j (a) and Huang-Rhys factor S_j (b) of each normal mode for 2ETPE, 2MTPE, 2STPE and 2OTPE in solution.
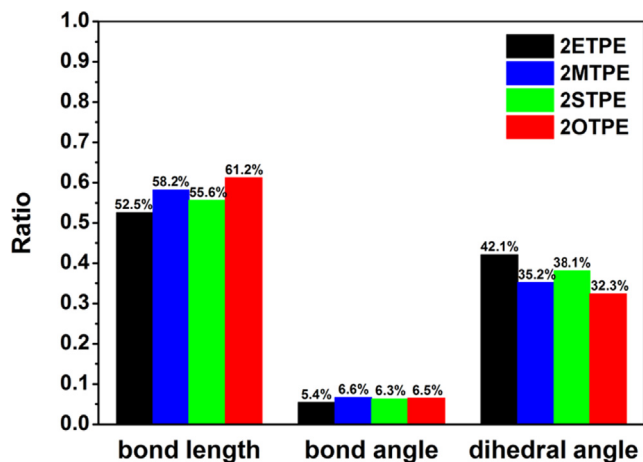

Fig. 5. Contributions from bond length, bond angle and dihedral angle to the total reorganization energy for 2ETPE, 2MTPE, 2STPE and 2OTPE in solution.

vibration in 2MTPE or 2STPE, and flapping vibration in 2OTPE.

Geometry relaxations onto internal coordinates are projected following Reimers [27]. Contributions from bond length, bond angle and dihedral angle are shown in Fig. 5. Notably, the contribution from dihedral angle to the total is 42.1% (283 meV) in 2ETPE, whereas it decreases to 38.1% (174 meV) in 2STPE, 35.2% (169 meV) in 2MTPE and 32.3% (117 meV) in 2OTPE, respectively. These results also reveal obviously from the molecular structure insight that the reduced reorganization energy upon shortening tethers mainly arises from the restricted out-of-plane vibrations, reflected by the suppressed variations

of the dihedral angles.

4. Conclusions

In summary, we have theoretically investigated the optical emission processes of several geminally locked TPE derivatives in solution combining the PCM method with the TVCF approach. We found that the calculated optical spectra of 2ETPE and 2OTPE agree well with the available experiments. The flexible 2ETPE has the largest k_{ic} value with 9 orders of magnitude, which quenches its emission. However, the better conjugation and stronger rigidity respectively accelerates the k_r and slows down the k_{ic} of 2OTPE, providing it with the highest Φ_f. The competition between the enhanced conjugation and attenuated rigidity of 2STPE compared to 2MTPE make them become moderately emissive luminogens with similar Φ_f. Through analyses of the non-radiative energy consumption channels, the electron-vibration couplings are found to decrease in the order of 2ETPE > 2STPE > 2MTPE > 2OTPE, which rationalizes the reduced k_{ic} in that order. Indeed, other excited-state decay paths [6,20] may also partly or all dissipate the energy due to the rather complex potential energy surface. We only simply emphasize one aspect that the out-of-plane vibrations are restricted with strengthening the tethers, which we believe is essential in the non-radiative decay pathways for such series of molecules. This theoretical study suggests that the optical properties of the TPE derivatives can be fine-tuned by modification of the tethers.

Finally, we note that the methodology we adopted here to study the excited-state decay processes are based on a displaced and distorted harmonic oscillator model among other approximations [28]. Song et al. have also pointed out the importance of considering the vibrational excitation influence and nucleus-electron interactions in the photoinduced electron transfer process [25], in addition to the non-radiative decay of the lowest excited state to the ground state mentioned in this work. Quantitative prediction of the optical emission properties from first-principles still consist of challenges [29].

Conflict of interest

There are no conflicts to declare.

Acknowledgement

References

[1] Z. Zhao, J.W.Y. Lam, B.Z. Tang, Tetraphenylethene: a versatile AIE building block for the construction of efficient luminescent materials for organic light-emitting diodes, J. Mater. Chem. 22 (2012) 23726–23740.

[2] D. Ding, K. Li, B. Liu, B.Z. Tang, Bioprobes based on AIE fluorogens, Acc. Chem. Res. 46 (2013) 2441–2453.

[3] Y.Q. Dong, J.W.Y. Lam, B.Z. Tang, Mechanochromic luminescence of aggregation-induced emission luminogens, J. Phys. Chem. Lett. 6 (2015) 3429–3436.

[4] J.D. Luo, Z.L. Xie, J.W.Y. Lam, L. Cheng, H.Y. Chen, C.F. Qiu, H.S. Kwok, X.W. Zhan, Y.Q. Liu, D.B. Zhu, B.Z. Tang, Aggregation-induced emission of 1-methyl-1,2,3,4,5-pentaphenylsilole, Chem. Commun. 1740–1741 (2001).

[5] N.L.C. Leung, N. Xie, W.Z. Yuan, Y. Liu, Q.Y. Wu, Q. Peng, Q. Miao, J.W.Y. Lam, B.Z. Tang, Restriction of intramolecular motions: the general mechanism behind aggregation-induced emission, Chem. Eur. J. 20 (2014) 15349–15353.

[6] Y. Cai, L. Du, K. Samedov, X. Gu, F. Qi, H.H.Y. Sung, B.O. Patrick, Z. Yan, X. Jiang, H. Zhang, J.W.Y. Lam, I.D. Williams, D. Lee Phillips, A. Qin, B.Z. Tang, Deciphering the working mechanism of aggregation-induced emission of tetraphenylethylene derivatives by ultrafast spectroscopy, Chem. Sci. 9 (2018) 4662–4670.

[7] J. Shi, N. Chang, C. Li, J. Mei, C. Deng, X. Luo, Z. Liu, Z. Bo, Y.Q. Dong, B.Z. Tang,

Locking the phenyl rings of tetraphenylethene step by step: understanding the mechanism of aggregation-induced emission, Chem. Commun. 48 (2012) 10675–10677.

[8] Y. Tapuhi, M.R. Suissa, S. Cohen, P.U. Biedermann, A. Levy, I. Agranat, The stereochemistry of overcrowded homomerous bistricyclic aromatic enes with alkylidene bridges, J. Chem. Soc., Perkin Trans. 2 (2000) 93–100.

[9] A. Levy, I. Agranat, Zinc-mediated reductive dimerizations of telluroxanthone and selenoxanthone. Tellurium–selenium selectivity, Tetrahedron Letters 41 (2000) 6157–6160.

[10] C. Adamo, V. Barone, Toward reliable density functional methods without adjustable parameters: the PBE0 model, J. Chem. Phys. 110 (1999) 6158–6170.

[11] D. Jacquemin, V. Wathelet, E.A. Perpète, C. Adamo, Extensive TD-DFT benchmark: singlet-excited states of organic molecules, J. Chem. Theory Comput. 5 (2009) 2420–2435.

[12] M.J. Frisch, G.W. Trucks, H.B. Schlegel, G.E. Scuseria, M.A. Robb, J.R. Cheeseman, G. Scalmani, V. Barone, G.A. Petersson, H. Nakatsuji, X. Li, M. Caricato, A.V. Marenich, J. Bloino, B.G. Janesko, R. Gomperts, B. Mennucci, H.P. Hratchian, J.V. Ortiz, A.F. Izmaylov, J.L. Sonnenberg, D. Williams-Young, F. Ding, F. Lipparini, F. Egidi, J. Goings, B. Peng, A. Petrone, T. Henderson, D. Ranasinghe, V.G. Zakrzewski, J. Gao, N. Rega, G. Zheng, W. Liang, M. Hada, M. Ehara, K. Toyota, R. Fukuda, J. Hasegawa, M. Ishida, T. Nakajima, Y. Honda, O. Kitao, H. Nakai, T. Vreven, K. Throssell, J.A. Montgomery Jr., J.E. Peralta, F. Ogliaro, M.J. Bearpark, J.J. Heyd, E.N. Brothers, K.N. Kudin, V.N. Staroverov, T.A. Keith, R. Kobayashi, J. Normand, K. Raghavachari, A.P. Rendell, J.C. Burant, S.S. Iyengar, J. Tomasi, M. Cossi, J.M. Millam, M. Klene, C. Adamo, R. Cammi, J.W. Ochterski, R.L. Martin, K. Morokuma, O. Farkas, J.B. Foresman, D.J. Fox, Gaussian16 Revision B.01, Gaussian Inc, Wallingford, CT, 2016.

[13] J. Tomasi, B. Mennucci, R. Cammi, Quantum mechanical continuum solvation models, Chem. Rev. 105 (2005) 2999–3094.

[14] R. Improta, V. Barone, G. Scalmani, M.J. Frisch, A state-specific polarizable continuum model time dependent density functional theory method for excited state calculations in solution, J. Chem. Phys. 125 (2006).

[15] M. Klessinger, J. Michl, Excited States and Photochemistry of Organic Molecules, VCH Publishers Inc, New York, USA, 2013.

[16] Y.L. Niu, W.Q. Li, Q. Peng, H. Geng, Y.P. Yi, L.J. Wang, G.J. Nan, D. Wang, Z.G. Shuai, MOlecular MAterials Property Prediction Package (MOMAP) 1.0: a software package for predicting the luminescent properties and mobility of organic

functional materials, Mol. Phys. 116 (2018) 1078–1090.

[17] Y.L. Niu, Q. Peng, C.M. Deng, X. Gao, Z.G. Shuai, Theory of excited state decays and optical spectra: application to polyatomic molecules, J. Phys. Chem. A 114 (2010) 7817–7831.

[18] Q. Peng, Y.P. Yi, Z.G. Shuai, J.S. Shao, Toward quantitative prediction of molecular fluorescence quantum efficiency: role of Duschinsky rotation, J. Am. Chem. Soc. 129 (2007) 9333–9339.

[19] S.H. Lin, Rate of interconversion of electronic and vibrational energy, J. Chem. Phys. 44 (1966) 3759–3767.

[20] Y.-J. Gao, X.-P. Chang, X.-Y. Liu, Q.-S. Li, G. Cui, W. Thiel, Excited-state decay paths in tetraphenylethene derivatives, J. Phys. Chem. A 121 (2017) 2572–2579.

[21] J.-B. Xiong, Y.-X. Yuan, L. Wang, J.-P. Sun, W.-G. Qiao, H.-C. Zhang, M. Duan, H. Han, S. Zhang, Y.-S. Zheng, Evidence for aggregation-induced emission from free rotation restriction of double bond at excited state, Org. Lett. 20 (2018) 373–376.

[22] K. Kokado, T. Machida, T. Iwasa, T. Taketsugu, K. Sada, Twist of C=C bond plays a crucial role in the quenching of AIE-active tetraphenylethene derivatives in solution, J. Phys. Chem. C 122 (2018) 245–251.

[23] H. Nie, K. Hu, Y. Cai, Q. Peng, Z. Zhao, R. Hu, J. Chen, S.-J. Su, A. Qin, B.Z. Tang, Tetraphenylfuran: aggregation-induced emission or aggregation-caused quenching? Mater. Chem. Front. 1 (2017) 1125–1129.

[24] Y.Q. Jiang, Q. Peng, X. Gao, Z.G. Shuai, Y.L. Niu, S.H. Lin, Theoretical design of polythienylenevinylene derivatives for improvements of light-emitting and photovoltaic performances, J. Mater. Chem. 22 (2012) 4491–4501.

[25] P. Song, Q. Zhou, Y. Li, F. Ma, M. Sun, Vibronic quantized tunneling controlled photoinduced electron transfer in an organic solar cell subjected to an external electric field, Phys. Chem. Chem. Phys. 19 (2017) 16105–16112.

[26] T. Zhang, W. Shi, D. Wang, S. Zhuo, Q. Peng, Z.G. Shuai, Pressure-induced emission enhancement in hexaphenylsilole: a computational study, J. Mater. Chem. C 7 (2019) 1388–1398.

[27] J.R. Reimers, A practical method for the use of curvilinear coordinates in calculations of normal-mode-projected displacements and Duschinsky rotation matrices for large molecules, J. Chem. Phys. 115 (2001) 9103–9109.

[28] Z.G. Shuai, Q. Peng, Excited states structure and processes: understanding organic light-emitting diodes at the molecular level, Phys. Rep. 537 (2014) 123–156.

[29] Z.G. Shuai, Q. Peng, Organic light-emitting diodes: theoretical understanding of highly efficient materials and development of computational methodology, Natl. Sci. Rev. 4 (2017) 224–239.